High-Q resonant modes in a finite array of dielectric particles

Evgeny N. Bulgakov[1,2] and Almas F. Sadreev[1]

[1]*Kirensky Institute of Physics, Federal Research Center KSC Siberian Branch, Russian Academy of Sciences, Krasnoyarsk 660036, Russia*

[2]*Siberian State Aerospace University, Krasnoyarsk 660014, Russia*

(Received 2 January 2019; published 26 March 2019)

We trace the Q factor of the resonant modes which are limited to bound states in the continuum (BICs) for $N = \infty$ in the finite array of N dielectric spheres and disks. For the symmetry-protected BICs we observe the quadratic dependence of the Q factor on N for high-refractive-index particles, while for low-refractive-index particles there is an interplay between the quadratic and cubic dependencies. The Q factor of accidental BICs grows cubically with N. We show that a plane wave can excite these quasi-BICs for tuning of the angle of incidence.

DOI: 10.1103/PhysRevA.99.033851

I. INTRODUCTION

Recently bound states in the radiation continuum (BICs) with zero Bloch vector were reported in infinitely long periodic arrays of dielectric cylinders in air [1–16] and on a substrate [11,15,17–24] (see also for the arrays of metallic wires on a substrate [25] and metal plates [26]). BICs propagating along the array were also shown to exist [5,14,27–32] as well as the BICs which can propagate along the cylinders [32,33], forming a new family of guided modes with frequencies above the light line. Among these periodic systems the one-dimensional arrays of spheres and disks are unique because of the axial symmetry that gives rise to the BICs with orbital angular momentum (OAM) [34–36], which is reflected in anomalous scattering of plane waves by the array, resulting in scattered electromagnetic fields with OAM propagating along the array [35,37,38]. Physically, the occurrence of BICs in the infinite array of dielectric particles is the result of the periodicity of the array that quantizes the radiation continua in the form of diffraction continua [5,38].

Obviously, infinite arrays of dielectric particles is an unrealistic limit. In practice, we deal with a finite number of N particles which have material losses given by the imaginary part of the refractive index, structural fluctuations of particles, the effect of substrate, etc., transforming the true BIC into a resonant mode with a small resonant width [22,36,38–41]. Although the full range of study of these factors is still far from completion, it was shown that the Q factor of the symmetry-protected quasi-BICs grows quadratically with N [36,40] and cubically for the accidental BICs [40]. First the cubic dependence $Q(N)$ was shown for the guided bound modes below the light line due to emission from the ends of the tight-binding chain [42,43]. Although the dependence $Q(N) \sim N^2$ was shown for the symmetry-protected (SP) BIC in the high-contrast disks [36], the case of the low-contrast particles does not obey this law, as we show here. The dependence $Q(N)$ for the non-symmetry-protected (accidental) BICs is cubic irrespective of the refractive of index of particles.

In the present paper we study $Q(N)$ of the resonant modes which are limited to the BICs for $N \to \infty$, both symmetry protected and accidental. Specifically, we consider finite arrays of dielectric spheres and coaxial disks. We reveal that the SP quasi-BICs radiate from the entire array while the accidental, quasi-BICs radiate only from the ends of the array. Also, we simulate radiation of resonant modes with use of a toy tight-binding chain, showing that coupling of the chain with the continuum results in different degrees of $Q(N)$. Moreover, the model reveals an important role of the value of coupling between dielectric particles which is inversely proportional to the refractive index of dielectric particles in the array. Because the group velocity of radiation is proportional to the bandwidth, i.e., the coupling between particles, we observe a clear tendency to enhance the Q factor with increasing the refractive index.

The phenomenon of enhancement of the Q factor was demonstrated by Rybin *et al.* [44], even for a single disk for variation of the aspect ratio, but the arrays of only a few dielectric rods show an extremely large Q factor [41]. A enhancement of the Q factor of dielectric nanoresonators is of a paramount interest and opens up new horizons for active and passive nanoscale all-dielectric devices.

II. RESONANT APPROXIMATION

The problem of scattering of electromagnetic waves by arrays of dielectric spheres can be formulated in the form of linear algebraic equations [34,35,37,38],

$$\widehat{L}\overrightarrow{\Psi} = \overrightarrow{\Psi}_{\rm inc}, \tag{1}$$

where the matrix $\widehat{L}$ is determined by a specific structure of dielectric particles, and the solution of this equation is given by the right-hand term, which is a source of electromagnetic waves. The specific form of the matrix $\widehat{L}$ and incident wave $\overrightarrow{\Psi}_{\rm inc}$ depends on a choice of the basis of specific representation. Respectively, for the case of spheres it is convenient to project the Maxwell equations onto the vector spherical functions specified by orbital momentum numbers l, m, where $m = -l, \ldots, l$ [34,35,38,45]. The incident wave can be TE/TM polarized with the electric and/or magnetic

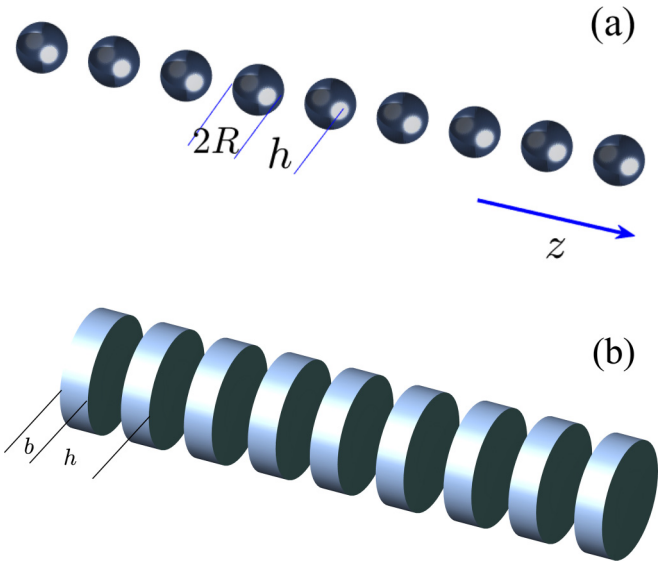

FIG. 1. Linear array of N (a) dielectric spheres and (b) disks.

field normal to the z-axis plane. We refer to the Appendix, where we present the matrix $\widehat{L}$ and incident wave $\vec{\Psi}_{\rm inc}$ for the case of a finite number of dielectric spheres.

On the other hand, there are solutions of the homogeneous equation

$$\widehat{L}\vec{\Psi} = 0 \tag{2}$$

which define the bound modes of the array. The solution of this equation with real frequency can be found only for the infinite periodical array comprising the bound states. For the finite arrays Eq. (2) can be solved by analytical continuation of the frequency whose imaginary part of the eigenfrequency defines the resonant width. In order to imagine the matrix elements of matrix $\widehat{L}$ we refer the reader to Refs. [34,45].

There might be two kinds of bound modes. The first type of mode has a wave number $\beta > k_0$ and describes guided waves along the array with wave number β and frequency k_0 below the light line. These solutions exist when the period of the array L is less than half of the wavelength $\lambda = 2\pi/k_0$ [42,45–47]. The second type of bound mode, with $\beta < k_0$, resides above the light cone to realize BICs [5,14,27–33]. In what follows we use dimensionless units, frequency $k_0 = \frac{\omega h}{c}$, and wave number along the array $\beta = k_z h$, where h is the distance between the dielectric particles in the array as shown in Fig. 1.

For the present problem it is important to note that $\widehat{L}$ is a square non-Hermitian matrix which can be defined in a biorthogonal basis of left and right eigenvectors,

$$\vec{y}_i\widehat{L} = \lambda_i\vec{y}_i,\ \widehat{L}\vec{x}_i = \lambda_i\vec{x}_i, \tag{3}$$

where $\vec{y}_i \cdot \vec{x}_j = \delta_{ij}$. Then the condition of completeness takes the following form:

$$\sum_i \vec{x}_i \cdot \vec{y}_i = 1, \tag{4}$$

from where one can write the following equalities,

$$\widehat{L} = \sum_i \lambda_i \vec{x}_i \vec{y}_i,\ \widehat{L}^{-1} = \sum_i \frac{\vec{x}_i \vec{y}_i}{\lambda_i}, \tag{5}$$

as well as the solution of Eq. (1),

$$\vec{\Psi} = \sum_i \frac{\vec{x}_i \vec{y}_i}{\lambda_i}\vec{\Psi}_{\rm inc}. \tag{6}$$

In what follows we are interested in high-Q eigenmodes which are limited to BICs for $N \to \infty$. In the linear periodic arrays with finite N these modes are distinguished by packing of an integer number of half wavelengths with corresponding frequencies proportional to $\pi n/N, n = 1, 2, 3, \ldots$ [36]. In what follows we focus on the lowest eigenmode whose corresponding complex eigenvalue λ_c is limited to zero with $N \to \infty$ to identify this mode as the SP BIC at the Γ point. We can consider this eigenmode to be the null eigenvector, as it follows from Eq. (2) [48], and write in the vicinity of resonant frequency

$$\lambda_c = iq[k_0 - k_{0c} + i\gamma_c], \tag{7}$$

where a small γ_c is responsible for weak leakage of this eigenmode with frequency k_{0c}. Expression (A11) is convenient for numerical calculation of the poles. Therefore the quasi-BIC mode dominates in the series (6)

$$\vec{\Psi} \approx -\frac{W_c}{q}\frac{i}{k_0 - k_{0c} + i\gamma_c}\vec{x}_c. \tag{8}$$

We then define the complex value

$$W_c = \vec{y}_c\vec{\Psi}_{\rm inc} \tag{9}$$

as the coupling constant of the incident wave with the resonant mode [49].

III. $Q(N)$ IN THE ARRAY OF SPHERES

We start consideration of the SP quasi-BICs in the finite arrays of dielectric spheres with $m = 0$. In Fig. 2(a) the true BIC solution with coefficients a_l^0 and b_l independent of cite index j in the series (A2) is shown [34], which transforms into the resonant mode with finite linewidth when N is restricted. The profile of one component of the EM field of this SP quasi-BIC with TM polarization is shown in Fig. 2(b) with coefficients $|b_l^0(j)|$ in Fig. 2(c), which shows that mainly the vector spherical functions with orbital quantum number $l = 2$ contribute to the resonant mode $\vec{y}_c$. For the case of TM polarization, the coefficients b_l^0 mostly contribute into the solution. In contrast to the case of an infinite array of spheres, there is also the contribution with $l = 1$. One can see that the SP quasi-BIC radiates from the whole array to give rise to the quadratic dependence of the Q factor on the number of spheres, as shown in Fig. 3(a), similar to the finite array of dielectric cylinders [40] and disks [36]. Therefore the case of spheres does not bring something new.

The accidental BIC shown in Fig. 4(a) also transforms into the quasi-BIC when the number of spheres is finite. However, the radiation power of the accidental quasi-BIC is smaller compared to the former SP quasi-BIC. Figure 4(b) reveals that the reason is the accidental quasi-BIC radiates mostly from

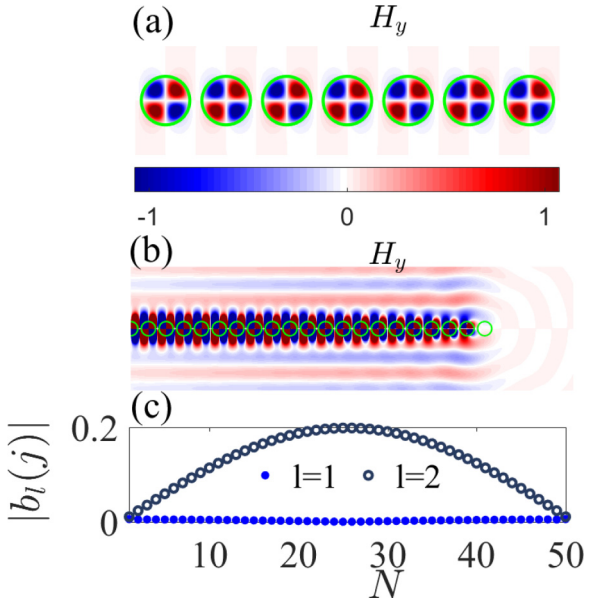

FIG. 2. Profile of the electromagnetic field for (a) of the SP BIC of TM polarization at the Γ point in the infinite periodic array of silica spheres with frequency $k_{0c} = 3.6026$ and (b) of the SP quasi-BIC of a finite array of 50 spheres with frequency $k_{0c} = 3.602\,15$. For clear resolution of the EM field profiles, we show only half of the array. (c) The coefficients of expansion in series (A2). The parameters of the spheres are $R = 0.4$, $\epsilon = 15$.

ends of the arrays, which enormously reduces the radiation losses compared to the SP quasi-BIC, as seen from Fig. 2(b). As a result, we obtain the cubic dependence of the Q factor on N, as Fig. 3(b) shows. Below we reproduce this cubic dependence by use of the tight-binding chain model coupled to the continuum at the ends of the chain.

At the end of this section we consider how these quasi-BICs are excited by incident plane waves. Figure 5 shows that the coupling, Eq. (9), of the SP quasi-BIC with the incident plane wave depends on the z component of wave vector β. One can see that the coupling decreases with increasing number of spheres, and the SP BIC is excited at discrete values $\beta = \pi(2n+1)/N$, $n = 0, 1, 2, \ldots$, including the normal incidence. The solid curve in Fig. 5 shows the maximal amplitude of the excited component of the EM field calculated numerically beyond the resonant approximation.

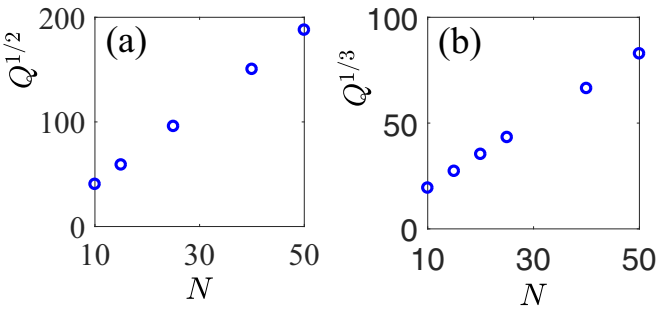

FIG. 3. Behavior of the Q factor as dependent on the number of spheres for the case of (a) SP quasi-BIC shown in Fig. 2(b) and (b) the accidental quasi-BIC shown in Fig. 4(b). $\epsilon = 15$.

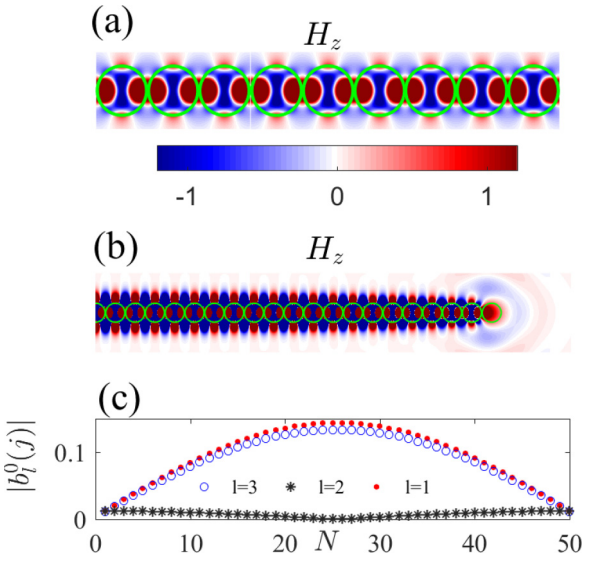

FIG. 4. Profile of the electromagnetic field H_z for (a) the accidental BIC with TE polarization and the frequency $k_0 = 2.9280$ at the Γ point in the infinite periodic array and (b) the accidental quasi-BIC with a $k_0 = 2.9283$ finite array of 50 silica spheres. (c) The coefficients of expansion in series (A2). The parameters of the spheres are $R = 0.481\,75$ and $\epsilon = 15$. For clear resolution of the EM field profiles, we show only half of the array.

The comparison shows that the resonant approximation well describes excitation of the SP quasi-BIC, but only for a small angle of incidence. As the angle increases, the resonant approximation worsens due to lack of resonant modes [50]. Figure 6 demonstrates that the plane wave strongly excites the SP quasi-BIC at $\beta = 0.09$ when the coupling of the plane

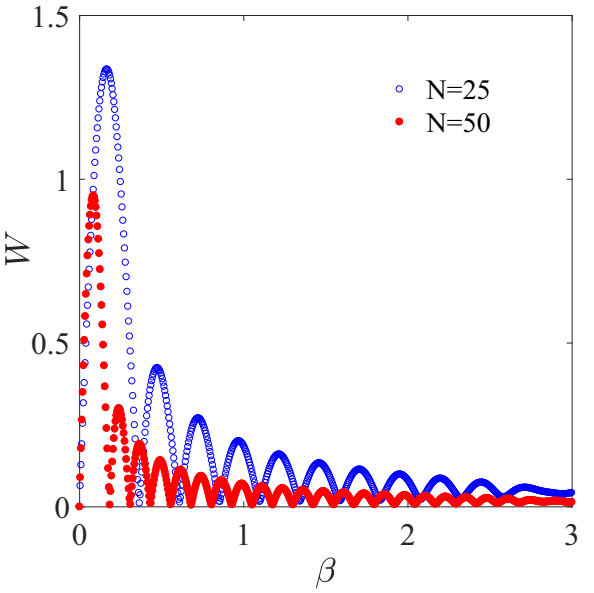

FIG. 5. Behavior of the coupling constant (9) as dependent on the angle of incidence for the case of the symmetry-protected quasi-BIC shown in Fig. 2: $k_0(N = 25) = 3.602$, $k_0(N = 50) = 3.602\,15$. Solid curve shows the maximal amplitude of excitation of the EM field by the TM plane wave in arbitrary units calculated numerically.

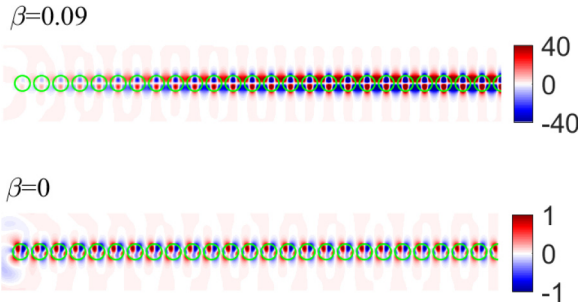

FIG. 6. Profile of H_z after excitation by TM plane wave with frequency $k_0 = 3.602\,15$ illuminating the array of 50 spheres at $\beta = 0.09$ and $\beta = 0$, which corresponds to maximal and minimal values of the coupling constant (9), shown in Fig. 5.

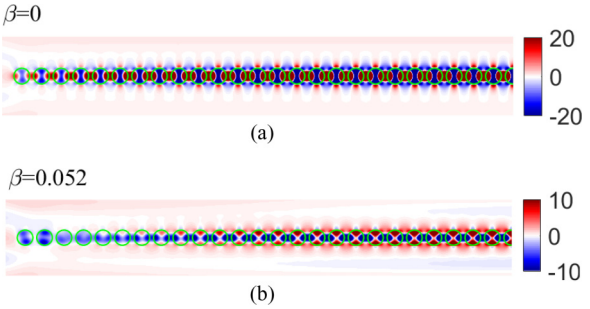

FIG. 8. Profile of E_z of the array of 50 spheres under illumination by a TE plane wave of frequency $k_0 = 3.9283$ at (a) $\beta = 0$ and (b) $\beta = 0.052$, which corresponds to maximal and minimal values of the coupling constant (9) shown in Fig. 7.

wave with the resonant mode is maximal, while at normal incidence of the plane wave we have weak excitation of all nonresonant modes of the array.

Figure 7 shows the oscillatory behavior of the coupling constant (9) of the accidental quasi-BIC with incident plane wave on the wave vector along array β. One can see that the coupling constant has almost constant peaks, which cardinally differs from the case of the SP quasi-BIC shown in Fig. 5. Profiles of component H_z excited by the plane wave are shown in Fig. 8 at two wave vector values, $\beta = 0$ and for the first minimum of the coupling constant (9) at $\beta = 0.052$, providing a clear indication of the maximal and minimal values of the coupling constant.

IV. $Q(N)$ IN THE ARRAY OF DISKS

While dielectric spheres have only one scale to tune, the radius of spheres compared to the period of the array, the disks bring two scales, the radius and thickness of disks. The array

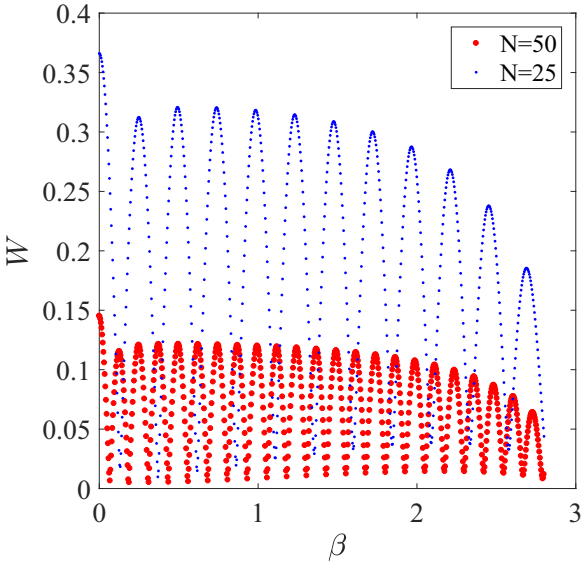

FIG. 7. Behavior of the coupling constant (9) as dependent on the wave vector β for the case of the accidental quasi-BIC shown in Fig. 4 under illumination by a TE plane wave with frequency $k_0 = 2.9283$.

of disks supports the BICs for both low and high refractive indices [35]. Note that the SP quasi-BICs were observed in the finite array of high-contrast ceramic disks [36]. In particular, it was established that the Q factor for the SP quasi-BIC grows quadratically with the number of disks but then saturates because of material losses in dielectric disks [36,39]. In this section we present results for the $Q(N)$ of quasi-BICs in the arrays of a finite number of dielectric disks by use of the method in the paper by Bigourdan *et al.* [51]. The results are collected in Table I, including the accidental quasi-BIC with orbital angular momentum $m = 1$, which is a hybridization of TE and TM polarizations.

We conclude from Table I the following. The resonant widths of SP quasi-BICs are superposed of two asymptotes, quadratic and cubic dependencies. This superposition is important for the low-contrast disks, in which for a number of disks less than 100 the cubic contribution is relevant. For the high-contrast disks the dependence is mostly quadratic, as was established for ceramic disks [36].

The important effect of the refraction index of the disks is related to a degree of localization of resonant modes inside of the disks, as demonstrated in Fig. 9. Let us consider the true SP BIC in the infinite array of dielectric disks at the Γ point. This BIC belongs to the leakage zone with resonant width $\mathrm{Im}(\mathrm{k}_0(\beta)) \sim \beta^2$ [32,52]. For a finite array the limiting wave number $\beta = \pi/N$ defines the SP quasi-BIC shown in Fig. 2, which results in a resonant width of $\mathrm{Im}[\mathrm{k}_0(\beta = \pi/\mathrm{N})] \sim \mathrm{N}^{-2}$ [36], as the last column of Table I evidences. Moreover, this substitution well agrees with the numerics quantitatively, as the second-to-last column of the table shows. As it will be shown below in the framework of the tight-binding chain, the dependence $Q(N)$ is directly related to coupling of the chain as a whole with the continuum.

Next, in the infinite array of dielectric infinitely long cylinders the unique case was shown when the accidental BIC guided at $\beta \neq 0$ collapses with the SP BIC for tuning of the radius of cylinders [31,32] and spheres [52]. Then the imaginary part of the radiating resonant mode in the leakage zone becomes proportional β^4 for the accidental BIC. In the array of disks we find a similar case of such a collapse and, respectively, the imaginary part of the radiating resonant mode in the leakage zone behaves as β^4, as presented in the third line of Table I. As a result, radiation from the whole array becomes

TABLE I. Parameters of quasi-BICs in an array of disks with thickness $b = 0.5$ and the period $h = 1$. Abbreviation SP means symmetry protected.

Type of BIC	k_0	R	ϵ	m	Re$[k_0(\beta)]$	–Im$[k_0(\beta)]$	–Im$[k_0(N)]$, numerics	–Im$[k_0(\beta=\pi/N)]$
SP TM	5.233	2.7	3	0	$0.785\beta^2$	$0.0247\beta^2$	$\frac{0.2795}{N^2}+\frac{35.66}{N^3}$	$\frac{0.244}{N^2}$
SP TE	3.8565	0.8	15	0	$-0.007\beta^2$	$0.0056\beta^2$	$\frac{0.0546}{N^2}+\frac{0.3}{N^3}$	$\frac{0.0553}{N^2}$
SP TM	5.4402	2.035	3	0	β^2	$0.02\beta^4$	$\frac{51.1}{N^3}$	
Accidental TM	4.8529	2.3633	3	0	$-0.766\beta^2$	$0.3\beta^4$	$\frac{55.66}{N^3}$	
Accidental hybrid	5.2987	2.0315	3	1	$0.533\beta^2$	$0.011\beta^2$	$\frac{0.094}{N^2}+\frac{19.2}{N^3}$	$\frac{0.11}{N^2}$

proportional $1/N^4$ to be neglected compared to the radiation from the ends of the array. Respectively, in the finite array of disks the corresponding quasi-BIC radiates from the ends of the array, as shown in Fig. 10(a), to give rise to $1/Q(N) \approx N^{-3}$, as shown in Table I. The fourth line in Table I shows the accidental quasi-BIC whose $Q(N)$ has the same cubic dependence as in the case of dielectric spheres. Figure 10(b) demonstrates that this accidental quasi-BIC from the fourth line of Table I radiates completely in the same manner as the quasi-BIC from the third line in Table I—from the ends of the array.

Finally, in the quasi-BIC with $m = 1$, which is a hybridization of SP quasi-BIC with TE polarization and accidental quasi-BIC with TM polarization [35], both quadratic and cubic dependencies contribute into $1/Q(N)$, as shown in the fifth line of Table I.

V. TIGHT-BINDING CHAIN

It is clearly seen from Figs. 4 and 9 that the SP quasi-BICs mostly radiate from all dielectric particles arranged linearly, while the accidental quasi-BICs radiate from the ends of the array. These numerical observations prompt us to use the simple one-dimensional tight-binding chain shown in Fig. 11, which has been successfully used for evaluation of the Q factor of guided modes below the light line [43] and the SP quasi-BICs at the Γ point above the light line [36]. The tight-binding Hamiltonian of the array of N particles has the following form:

$$\widehat{H}_B = -u\sum_{j=1}^{N-1}\psi_j\psi_{j+1}^* + \text{H.c.} \tag{10}$$

The eigenmodes and the eigenlevels of the array are

$$\psi_n(j) = \sqrt{\frac{2}{N+1}}\sin(k_n j), \tag{11}$$

$$E_n = 2u(1-\cos k_n),$$

$$k_n = \frac{\pi n}{N+12}, n = 1, 2, 3, \ldots, N. \tag{12}$$

A semi-infinite waveguide below the chain in Fig. 11(a) models the radiation continuum which supports the propagating modes,

$$\psi_p(j_x, j_y) = \sqrt{\frac{1}{2\pi\sin k}}\sqrt{\frac{2}{N+1}}\sin\left(\frac{\pi p j_y}{N+1}\right)e^{ik_p j_x}, \tag{13}$$

with the spectra

$$E = 4 - 2\cos k_p - 2\cos[\pi p/(N+1)],\ p = 1, 2, 3, \ldots, \tag{14}$$

with a propagation band from 0 to 4. Moreover, we suppose each particle is coupled with the radiation continuum through the coupling matrix element v. Next we assume that the wave in the first channel $p = 1$ is propagating over the wide waveguide (radiation continuum) and is scattering by the chain. Then the scattering in the first channel $p = 1$ is given

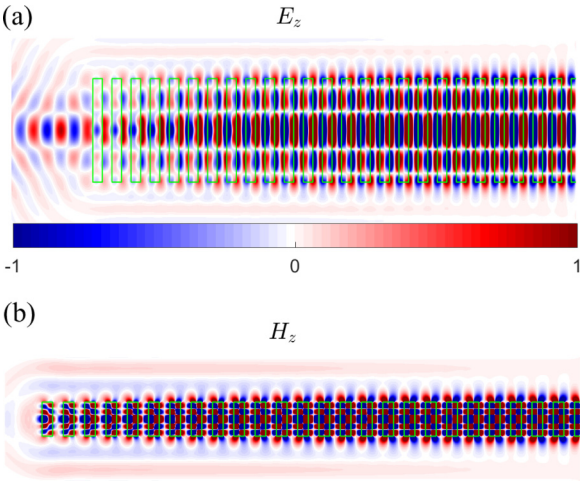

FIG. 9. Profile of EM field of resonant modes corresponding SP quasi-BICs in an array of 50 disks with (a) $\epsilon = 3$ (the first line in Table I) and (b) $\epsilon = 15$ (the second line in Table I).

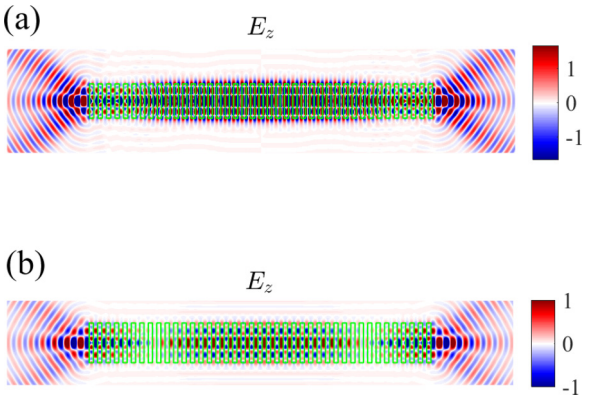

FIG. 10. Profiles of EM field of (a) SP quasi-BIC (the third line in Table I) and (b) accidental quasi-BIC (the fourth line in Table I) in an array of 41 disks.

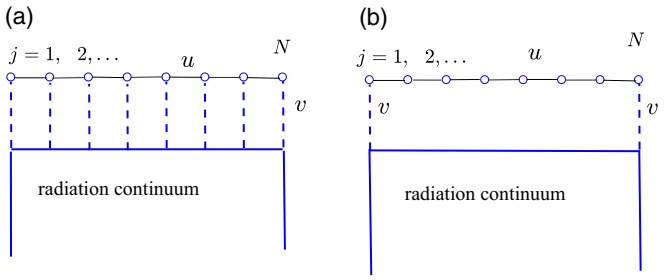

FIG. 11. Tight-binding simulation of N particles coupled to a wide waveguide simulating the radiation continuum via the coupling constant v.

by the Green's function with the transmission amplitude

$$T = 2iv^2 \sin k_1 \sum_{jj'} \psi_1(j) G(j, j') \psi_1(j'), \tag{15}$$

where the Green's function is given by the inverse of the effective non-Hermitian Hamiltonian [53,54]

$$\widehat{G} = \frac{1}{E + i0 - \widehat{H}_{\text{eff}}} \tag{16}$$

and $\psi_1(j) = \sqrt{\frac{2}{N+1}} \sin(\frac{\pi j}{N+1}), j=1,2,\ldots,N$.

For the case of the SP quasi-BIC with the eigenmode $\psi_1(j)$, all N sites are coupled with the radiation continuum via the coupling constant v, as shown in Fig. 11(a), which defines the effective Hamiltonian as follows:

$$\widehat{H}_{\text{eff}} = \widehat{H}_B - v^2 \sum_p \exp(ik_p), \tag{17}$$

giving rise to the linewidth $\Gamma \sim v^2 \frac{1}{N} \frac{\pi^2}{N^2} N \sim \frac{1}{N^2}$ and therefore $Q(N) \sim N^2$. The transmission spectra is shown in Fig. 12. One can see that two edge resonances, the first and the Nth have extremely small widths which are proportional to the coupling constant u between sites (disks) for small u but fast saturates with growth of u as shown in Fig. 13.

The accidental quasi-BIC radiate only from the ends of the arrays, which is modelled by all coupling matrix elements v

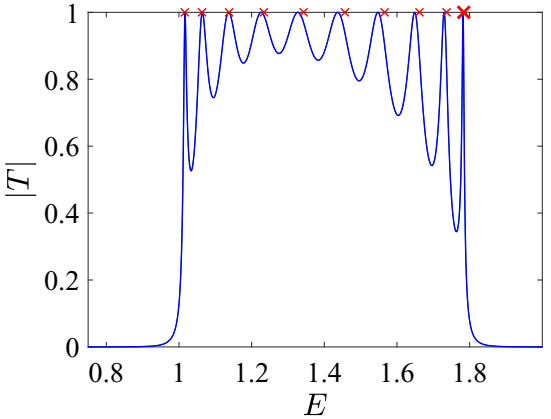

FIG. 12. Transmission spectra of an array of 10 sites. Crosses mark the eigenlevels of the model given by Eq. (12), with $E_g = 1$, $u = 0.2$, $v = 0.4$.

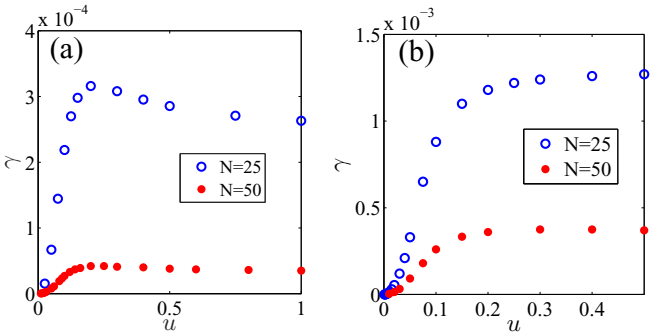

FIG. 13. The resonant width of the first resonant peak in the transmission spectra shown in Fig. 12 vs u for coupling of the tight-binding chain with the continuum by (a) all cites [Fig. 11(a)] and (b) only edge cites of the chain [Fig. 11(b)].

being equal to zero, except for the first and Nth sites, as shown in Fig. 11(b). Then the effective non-Hermitian Hamiltonian will take the following form:

$$\widehat{H}_{\text{eff}} = \widehat{H}_B - v^2 \sum_p \exp(ik_p), \text{ if } j = 1, N, \tag{18}$$

otherwise, $\widehat{H}_{\text{eff}} = \widehat{H}_B$. Then the resonant width is defined as $\Gamma = -2Im(z_1)$, where $z_\lambda, \lambda = 1, 2, 3, \ldots, N$ are the complex eigenvalues of $\widehat{H}_{\text{eff}}$ [54,55]. This resonant width corresponds to the half-width of the first resonant peak in the transmittance in Fig. 12, marked by the larger red x. Therefore we can evaluate the resonant width $\Gamma \sim v^2 \frac{1}{N} \frac{\pi^2}{N^2} \sim \frac{1}{N^3}$ because of the leakage of the radiation only from the ends of the chain, as shown in Fig. 11(b). Thus we have the dependence $Q(N) \sim N^3$ shown in Fig. 14, which is surprisingly independent of the width of band $2u$. The dependence N^3 can be easily understood from Eq. (11). A similar result was established by Polishchuk *et al.* [43] for the bound modes below the light line. Figure 14 also shows the important role of the propagation band of the chain with regard to Q factor, as Taghizadeh and Chung first reported [41]. One can conclude that with a tendency to flat bands the quasi-BIC are limited to the compact-BICs that were reported recently [56]. Physically that tendency is related to the fact that the group velocity of radiation of quasi-BICs in the chain is limited to zero when $u \to 0$ [57].

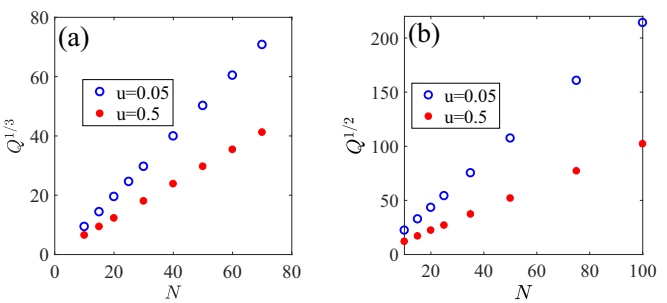

FIG. 14. Q factor of the tight-binding chain vs N for coupling of the tight-binding chain with the continuum by (a) all cites [Fig. 11(a)] and (b) only edge cites of the chain [Fig. 10(b)].

VI. SUMMARY AND CONCLUSIONS

The BICs exist only in the infinite periodic array of dielectric particles. In the array of a finite number of particles, the BICs become resonant modes with small but finite resonant width (quasi-BICs). There are two different cases, the case of the SP quasi-BICs and accidental quasi-BICs. The last occur for tuning of particle parameters, for example, of radius of spheres [5] or disks [35].

The case of the SP quasi-BICs is sensitive to the choice of particles and their refraction index. The greater refractive index of disks the more localization of resonant modes inside of the disks and the less the coupling between the neighbor disks. Respectively, the less the group velocity of leakage of the resonant mode, the higher the Q factor [41]. That tendency of increasing the Q factor was verified by use of tight-binding chain models. As seen from Table I, the dependence $Q(N)$ in the SP quasi-BICs in the array of disks shows an interplay between the quadratic and cubic dependencies. The cubic contribution becomes important for particles with low-refractive particles. In the high-refractive-index disks we have mainly the quadratic dependence of $Q(N)$, as it was established theoretically [38–40] and experimentally [36]. That law is the result of the SP quasi-BIC radiating from the whole array of particles. However, for the case of low-refractive-index particles, the cubic contribution in $Q(N)$ also becomes important.

In the array of dielectric particles, the accidental quasi-BIC leakages mostly occur from the edges of the finite chain of particles, as Fig. 10 illustrates, to give rise to the Q factor proportional to the cubic number of particles. That asymptote does not depend on the type of particles and their refraction index. However, for the accidental quasi-BICs with OAM $m \neq 0$ with hybridized polarizations, a small fracture of the quadratic dependence on $Q(N)$ arises. The reason is because the BICs with $m \neq 0$ are a hybridization of SP BIC for TM polarization and accidental BIC for TE polarization [35].

ACKNOWLEDGMENTS

We acknowledge discussions with D. N. Maksimov. This work was partially supported by the Ministry of Education and Science of the Russian Federation (State Contract No. 3.1845.2017) and RFBR Grant No. 19-02-00055.

APPENDIX

The incident plane wave can be written as well as the solution of the scattering problem for the electromagnetic field [Eq. (1)] of vector spherical functions [58] $\mathbf{M}_{lm}$, $\mathbf{N}_{lm}$:

$$\vec{\Psi} = \begin{pmatrix} \vec{E} \\ \vec{H} \end{pmatrix}^{\sigma} = \sum_{l=1}^{\infty} \sum_{m=-l}^{l} \left[p_{lm}^{\sigma} \begin{pmatrix} \mathbf{N}_{lm} \\ -i\sqrt{\epsilon}\mathbf{M}_{lm} \end{pmatrix} + q_{lm}^{\sigma} \begin{pmatrix} \mathbf{M}_{lm} \\ -i\sqrt{\epsilon}\mathbf{N}_{lm} \end{pmatrix} \right], \tag{A1}$$

$$\begin{aligned} \mathbf{E}(\mathbf{r}) &= \sum_{j} \sum_{lm} [a_{lm}(j)\mathbf{M}_{lm}(\mathbf{r} - \mathbf{R}_j) + b_{lm}(j)\mathbf{N}_{lm}(\mathbf{r} - \mathbf{R}_j)], \\ \mathbf{H}(\mathbf{r}) &= -i \sum_{j} \sum_{lm} [a_{lm}(j)\mathbf{N}_{lm}(\mathbf{r} - \mathbf{R}_j) + b_{lm}(j)\mathbf{M}_{lm}(\mathbf{r} - \mathbf{R}_j)], \end{aligned} \tag{A2}$$

where σ specifies polarization of the electromagnetic field, $\mathbf{R}_j$ the response for positions of centers of spheres, l can be defined as orbital momentum, and m as its projection onto the z axis. The dependence of coefficients $a_{lm}(j)$, $b_{lm}(j)$ on sites j corresponds for a finite number of spheres. Due to the axial symmetry of the array of spheres, the solution of Eq. (2) for the resonant mode can be fixed by orbital angular momentum number m. Then Eq. (2) can be written as follows [34,45]:

$$\begin{aligned} a_{lm}(j) &= Z_{TE,l} \sum_{l'} \sum_{j \neq j'} \left[a_{l'm}(j') \mathcal{A}_{ll'}^{mm}(j - j') + b_{l'm} \mathcal{B}_{ll'}^{mm}(j - j') \right], \\ b_{lm} &= Z_{TM,l} \sum_{l'} \sum_{j \neq j'} \left[a_{l'm}(j') \mathcal{B}_{ll'}^{mm}(j - j') + b_{l'm} \mathcal{B}_{ll'}^{mm}(j - j') \right]. \end{aligned} \tag{A3}$$

The Lorenz-Mie coefficients $Z_{TE,l}$ and $Z_{TM,l}$ are derived in a book by Stratton [58] as follows:

$$\begin{aligned} Z_{TE,l} &= \frac{j_l(kR)[r j_l(k_0 r)]'_{r=R} - j_l(k_0 R)[r j_l(kr)]'_{r=R}}{h_l(k_0 R)[r j_l(kr)]'_{r=R} - j_l(kR)[r h_l(k_0 r)]'_{r=R}}, \\ Z_{TM,l} &= \frac{\epsilon j_l(kR)[r j_l(k_0 r)]'_{r=R} - j_l(k_0 R)[r j_l(kr)]'_{r=R}}{h_l(k_0 R)[r j_l(kr)]'_{r=R} - \epsilon j_l(kR)[r h_l(k_0 r)]'_{r=R}}, \end{aligned} \tag{A4}$$

where $k = \sqrt{\epsilon} k_0$ and ϵ is the dielectric constant of the spheres. For the infinite array of spheres the matrix elements $\mathcal{A}_{ll'}^{mm}$, $\mathcal{B}_{ll'}^{mm}$ were independent of the site index j. For the finite array [45],

$$\mathcal{A}_{ll'}^{mm}(j) = 4\pi(-1)^m i^{l'-l} \sqrt{\frac{l'(l'+1)}{l(l+1)}} \sum_{p=|l-l'|;l+l'+p \text{ even}}^{l+l'} g_{ll'p} \mathcal{G}(l, m; l', -m; p) h_p(k|js|) \lambda_{p0}(-i \operatorname{sgn}(j))^p, \tag{A5}$$

$$\mathcal{B}_{ll'}^{mm} = \frac{2\pi(-1)^m i^{l'-l}}{\sqrt{l(l+1)l'(l'+1)}} \sum_{p=|l-l'|+1;l+l'+p \text{ odd}}^{l+l'-1} \sqrt{\frac{2p+1}{2p-1}} \mathcal{H}(l,m;l',-m;p) h_p(k|js|) \lambda_{p0}(-i\,\mathrm{sgn}(j))^p, \tag{A6}$$

where $h_p(x)$ are the spherical Hankel functions. The coefficients

$$g_{ll'p} = 1 + \frac{(l-l'+p+1)(l+l'-p)}{2l'(2l'+1)} - \frac{(l'-l+p+1)(l+l'+p+2)}{2(l'+1)(2l'+1)}, \tag{A7}$$

$$\mathcal{G}(l,m;l',m';p) = \frac{(-1)^{m+m'}}{\sqrt{4\pi}} \sqrt{(2l+1)(2l'+1)(2p+1)} \begin{pmatrix} l & l' & p \\ m & m' & -m-m' \end{pmatrix} \begin{pmatrix} l & l' & p \\ 0 & 0 & 0 \end{pmatrix}, \tag{A8}$$

are expressed in terms of the Wigner 3-j symbols,

$$\mathcal{H}(l,m;l',-m;p) = \sum_{s=-1}^{1} \mathcal{G}_s(l,m;l',-m;p), \tag{A9}$$

with

$$\begin{aligned} \mathcal{G}_0(l,m;l',-m;p) &= -2m|p|\mathcal{G}(l,m;l',-m;p-1), \\ \mathcal{G}_{\pm1}(l,m;l',-m;p) &= \mp\sqrt{(l'\pm m)(l'\mp m+1)p(p-1)}\mathcal{G}(l,m;l',-m\pm1;p-1), \end{aligned} \tag{A10}$$

and

$$\lambda_{lm} = \sqrt{\frac{(2l+1)(l-m)!}{4\pi(l+m)!}}. \tag{A11}$$

[1] S. P. Shipman and S. Venakides, Phys. Rev. E **71**, 026611 (2005).
[2] S. P. Shipman, J. Ribbeck, K. H. Smith, and C. Weeks, IEEE Photon. J. **2**, 911 (2010).
[3] D. C. Marinica, A. G. Borisov, and S. V. Shabanov, Phys. Rev. Lett. **100**, 183902 (2008).
[4] S. Weimann, Y. Xu, R. Keil, A. E. Miroshnichenko, A. Tünnermann, S. Nolte, A. A. Sukhorukov, A. Szameit, and Y. S. Kivshar, Phys. Rev. Lett. **111**, 240403 (2013).
[5] E. N. Bulgakov and A. F. Sadreev, Phys. Rev. A **90**, 053801 (2014).
[6] J. M. Foley, S. M. Young, and J. D. Phillips, Phys. Rev. B **89**, 165111 (2014).
[7] Zhen Hu and Ya Yan Lu, J. Opt. **17**, 065601 (2015).
[8] M. Song, H. Yu, C. Wang, N. Yao, M. Pu, J. Luo, Z. Zhang, and X. Luo, Opt. Express **23**, 2895 (2015).
[9] J. W. Yoon, S. H. Song, and R. Magnusson, Sci. Rep. **5**, 18301 (2015).
[10] Z. Wang, H. Zhang, L. Ni, W. Hu, and C. Peng, IEEE J. Quant. Electron. **52**, 1 (2016).
[11] L. Ni, Z. Wang, C. Peng, and Z. Li, Phys. Rev. B **94**, 245148 (2016).
[12] L. Yuan, Opt. Quantum Electron. **48**, 182 (2016).
[13] L. Yuan and Y. Y. Lu, Opt. Lett. **42**, 4490 (2017).
[14] L. Yuan and Y. Y. Lu, J. Phys. B: At. Mol. Opt. Phys. **50**, 05LT01 (2017).
[15] Z. Hu and Y. Y. Lu, J. Phys. B: At. Mol. Opt. Phys. **51**, 035402 (2017).
[16] L. Yuan and Y. Y. Lu, Phys. Rev. A **97**, 043828 (2018).
[17] C. W. Hsu, B. Zhen, J. Lee, S. G. Johnson, J. D. Joannopoulos, and M. Soljačić, Nature (London) **499**, 188 (2013).
[18] C. W. Hsu, B. Zhen, A. D. Stone, J. D. Joannopoulos, and M. Soljačić, Nat. Rev. Mater. **1**, 16048 (2016).
[19] M. Niraula, J. W. Yoon, and R. Magnusson, Opt. Express **23**, 23428 (2015).
[20] Y. Wang, J. Song, L. Dong, and M. Lu, J. Opt. Soc. Am. B **33**, 2472 (2016).
[21] Z. F. Sadrieva and A. A. Bogdanov, J. Phys.: Conf. Series **741**, 012122 (2016).
[22] Z. F. Sadrieva, I. S. Sinev, K. L. Koshelev, A. Samusev, I. V. Iorsh, O. Takayama, R. Malureanu, A. A. Bogdanov, and A. V. Lavrinenko, ACS Photonics **4**, 723 (2017).
[23] E. N. Bulgakov, D. N. Maksimov, P. N. Semina, and S. A. Skorobogatov, J. Opt. Soc. Am. B **35**, 1218 (2018).
[24] S.-G. Lee and R. Magnusson, Phys. Rev. B **99**, 045304 (2019).
[25] S. G. Tikhodeev, A. L. Yablonskii, E. A. Muljarov, N. A. Gippius, and T. Ishihara, Phys. Rev. B **66**, 045102 (2002).
[26] W. Zhang, A. Charous, M. Nagai, D. M. Mittleman, and R. Mendis, Opt. Express **26**, 13195 (2018).
[27] C.-L. Zou, J.-M. Cui, F.-W. Sun, X. Xiong, X.-B. Zou, Z.-F. Han, and G.-C. Guo, Laser Photon. Rev. **9**, 114 (2015).
[28] X. Gao, C. W. Hsu, B. Zhen, X. Lin, J. D. Joannopoulos, M. Soljačić, and H. Chen, Sci. Rep. **6**, 31908 (2016).
[29] E. N. Bulgakov and D. N. Maksimov, Opt. Lett. **41**, 3888 (2016).
[30] Z. Hu and Y. Y. Lu, J. Opt. Soc. Am. B **34**, 1878 (2017).
[31] E. N. Bulgakov and D. N. Maksimov, Phys. Rev. Lett. **118**, 267401 (2017).
[32] E. N. Bulgakov and D. N. Maksimov, Phys. Rev. A **96**, 063833 (2017).
[33] B. Zhen, C. W. Hsu, L. Lu, A. D. Stone, and M. Soljačić, Phys. Rev. Lett **113**, 257401 (2014).

[34] E. N. Bulgakov and A. F. Sadreev, Phys. Rev. A **92**, 023816 (2015).
[35] E. N. Bulgakov and A. F. Sadreev, Phys. Rev. A **96**, 013841 (2017).
[36] M. Balyzin, Z. Sadrieva, M. Belyakov, P. Kapitanova, A. Sadreev, and A. Bogdanov, J. Phys.: Conf. Ser. **1092**, 012012 (2018).
[37] E. N. Bulgakov and A. F. Sadreev, Phys. Rev. A **94**, 033856 (2016).
[38] E. N. Bulgakov and A. F. Sadreev, Adv. Electromag. **6**, 1 (2017).
[39] C. P. Liangfu Ni, J. Jin, and Z. Li, Opt. Express **25**, 5580 (2017).
[40] E. Bulgakov and D. N. Maksimov, Opt. Express **25**, 14134 (2017).
[41] A. Taghizadeh and I.-S. Chung, App. Phys. Lett. **111**, 031114 (2017).
[42] G. S. Blaustein, M. I. Gozman, O. Samoylova, I. Y. Polishchuk, and A. L. Burin, Opt. Express **15**, 17380 (2007).
[43] I. Y. Polishchuk, A. A. Anastasiev, E. A. Tsyvkunova, M. I. Gozman, S. V. Solov'ov, and Y. I. Polishchuk, Phys. Rev. A **95**, 053847 (2017).
[44] M. V. Rybin, K. L. Koshelev, Z. F. Sadrieva, K. B. Samusev, A. A. Bogdanov, M. F. Limonov, and Y. S. Kivshar, Phys. Rev. Lett. **119**, 243901 (2017).
[45] C. Linton, V. Zalipaev, and I. Thompson, Wave Motion **50**, 29 (2013).
[46] A. L. Burin, H. Cao, G. C. Schatz, and M. A. Ratner, J. Opt. Soc. Am. B **21**, 121 (2004).
[47] J. Du, S. Liu, Z. Lin, J. Zi, and S. T. Chui, Phys. Rev. A **79**, 051801(R) (2009).
[48] E. N. Bulgakov, K. N. Pichugin, A. F. Sadreev, and I. Rotter, JETP Lett. **84**, 430 (2006).
[49] E. N. Bulgakov, I. Rotter, and A. F. Sadreev, Phys. Rev. A **75**, 067401 (2007).
[50] P. Lalanne, W. Yan, K. Vynck, C. Sauvan, and J.-P. Hugonin, Laser Photonics Rev. **12**, 1700113 (2018).
[51] F. Bigourdan, J.-P. Hugonin, and P. Lalanne, J. Opt. Soc. Am. A **31**, 1303 (2014).
[52] E. N. Bulgakov and D. N. Maksimov, J. Opt. Soc. Am. B **35**, 2443 (2018).
[53] S. Datta, *Electronic Transport in Mesoscopic Systems* (Cambridge University Press, Cambridge, England, 1995).
[54] A. Sadreev and I. Rotter, J. Phys. A: Math. Gen. **36**, 11413 (2003).
[55] M. P. J. Okołowicz and I. Rotter, Phys. Rep. **374**, 271 (2003).
[56] M. Röntgen, C. V. Morfonios, and P. Schmelcher, Phys. Rev. B **97**, 035161 (2018).
[57] M. Ibanescu, S. G. Johnson, D. Roundy, Y. Fink, and J. D. Joannopoulos, Opt. Lett. **30**, 552 (2005).
[58] J. A. Stratton, *Electromagnetic Theory* (McGraw-Hill Book Company, Inc., New York, 1941).